MORE-SPARKLING: non-cartesian trajectories with minimized off-resonance effects

Chaithya Giliyar Radhakrishna, Guillaume Daval-Frérot, Aurélien Massire, Boris Mailhé, Mariappan Nadar, Alexandre Vignaud, Philippe Ciuciu

MORE-SPARKLING: Non-Cartesian trajectories with Minimized Off-Resonance Effects

Chaithya G R*[1,2], Guillaume Daval-Frérot*[1,2,3], Aurélien Massire[3], Boris Mailhe[3,4], Mariappan Nadar[3,4], Alexandre Vignaud[1], and Philippe Ciuciu[1,2]

[1]CEA, Joliot, NeuroSpin, Université Paris-Saclay, F-91191 Gif-sur-Yvette, France
[2]Inria, Parietal, Université Paris-Saclay, F-91120 Palaiseau, France
[3]Siemens Healthcare SAS, Saint-Denis, 93210, France
[4]Siemens Healthineers, Princeton, 08540, NJ, USA

Synopsis

We augment the recently introduced SPARKLING algorithm and propose an improved mathematical formulation that takes the temporal dependence of the MR signal into account. This prevents the trajectories from sampling similar portions of k-space at different times, thereby reducing distortions and blurring induced by B_0 inhomogenieties. Overall, these trajectories present a smooth distribution over time in k-space and Minimized Off-Resonance Effects (MORE-SPARKLING), verified both retrospectively and prospectively with scans performed in vivo at 3T on a healthy volunteer.

Summary of main findings

New trajectories result in minimized off-resonance artifacts with 3dB gain in PSNR with retrospective studies. In prospective scans at 15-fold acceleration, they permit recovery of the signal dropouts observed on original SPARKLING acquisitions at larger B_0 field inhomogenieties.

1 Introduction

Reducing the scan time in MRI while preserving the highest image quality has been a longstanding goal within the MR community. According to compressed

sensing theory, k-space can be optimally undersampled through variable density sampling. Recently, the SPARKLING[6] algorithm was introduced to generate sampling patterns that cover the k-space according to a prescribed target sampling distribution (TSD) whereby each k-space trajectory satisfied the MR hardware constraints. This method was successfully extended to 3D,[1,7] however the presence of amplified patient-induced ΔB_0 artifacts was observed.[1] While the B_0 field inhomogeneities can be addressed through post-processing with correction methods[4] without additional scans,[2] it seems possible to mitigate their impact with improved design of the trajectories.

In this work, we incorporate additional components of the MR signal in the formulation of the SPARKLING optimization problem and produce trajectories with Minimized Off-Resonance Effects (MORE) in the final reconstructed MR image.

2 Theory

Following the original formulation,[1] a k-space sampling pattern $\mathbf{K} = (\mathbf{k}_i)_{i=1}^{N_c}$ is composed of N_c shots, with each 3D shot composed of N_s samples acquired over the readout duration such that $\mathbf{k}_i(t) = (k_{i,x}(t), k_{i,y}(t), k_{i,z}(t))$. The trajectory $\mathbf{K}$ is optimized[1,6] as:

$$\widehat{\mathbf{K}} = \underset{\mathbf{K}\in\mathcal{Q}^{N_c}}{\arg\min}\, F_p(\mathbf{K}) = F_p^{\mathrm{a}}(\mathbf{K}) - F_p^{\mathrm{r}}(\mathbf{K}) \tag{1}$$

with $p = N_c \times N_s$ samplings points, $\mathcal{Q}^{N_c}$ the N_c-dimensional set of feasible shots that meet the MR hardware constraints ([1, Eq.(2)]), $F_p^{\mathrm{a}}(\mathbf{K})$ the attraction term which ensures the sampling pattern $\mathbf{K}$ follows a prescribed TSD ρ and $F_p^{\mathrm{r}}(\mathbf{K})$ the repulsion term to avoid clumping of samples. From [1, Eq.(5)], we obtain $F_p^{\mathrm{r}}(\mathbf{K})$ as:

$$F_p^{\mathrm{r}}(\mathbf{K}) = \frac{1}{2p^2} \sum_{1\leq i,j\leq p} ||\mathbf{K}[i] - \mathbf{K}[j]||_2 \tag{2}$$

Ideally, the measured k-space samples $\mathbf{Y} = (\mathbf{y}_j)_{j=1}^{N_c}$ are given by:

$$\mathbf{y}_j(t) = \int \mathbf{x}_{\boldsymbol{r}}\, e^{-(\alpha_{\boldsymbol{r}} + \imath\omega_{\boldsymbol{r}})t} e^{-2\imath\pi(\mathrm{k}_j(t)\cdot\boldsymbol{r})} d\boldsymbol{r} \tag{3}$$

with $\mathbf{x}_{\mathbf{r}}$ the transverse magnetization of the object, $\alpha_{\boldsymbol{r}}$ the T_2^* decay and $\omega_{\boldsymbol{r}}$ the off-resonance at voxel $\boldsymbol{r}$. Note the temporal dependence of $\mathbf{Y}$ on $\alpha_{\boldsymbol{r}}$ and $\omega_{\boldsymbol{r}}$, not considered in the original SPARKLING formulation. This results in trajectories that may be locally inconsistent because close samples may be collected at different times (Fig.1(A)), leading to amplified ΔB_0 artifacts as observed in [1, Fig.S6].

3 Methods

We propose to mitigate the impact of B_0 inhomogeneities by adding the following temporal weights in the repulsion term $F_p^{\mathrm{r}}(\mathbf{K})$ as:

$$F_p^{\mathrm{r}}(\mathbf{K}) = \frac{1}{2p^2} \sum_{1 \leq i,j \leq p} e^{|t_i - t_j|} ||\mathbf{K}[i] - \mathbf{K}[j]||_2 \tag{4}$$

where t_i and t_j correspond to the times when the samples $\mathbf{K}[i]$ and $\mathbf{K}[j]$ are acquired. Note that $e^{|t_i - t_j|} \geq 1$, thereby increasing the repulsion term between temporally spaced out points. While generating the modified trajectories, large k-space holes are observed in Fig.1(B) as increased repulsion occurs in regions where the trajectories that start and end nearly at the same location along a plane. To address this issue, we benefited from the multi-resolution sampling design implemented in SPARKLING [1, Sec.II-E] which starts by spreading $p_{i_{\max}} = p/2^{i_{\max}}$ samples at the maximal $i_{\max} = 5$ decimation levels and iterates through a dyadic process, i.e. $p_{i_{\max}-i} = 2^i p_{i_{\max}}$ for $i = 1:5$ ($p_0 = p$). Here, we introduce the temporal weighting in the optimization process, and we call $TW_i,\ i = 0:2$, when this weighting is activated up to to the decimation step i with $p_{i_{\max}-i}$ samples. This results in significantly reduced k-space holes for TW_1 and TW_2 as presented in Fig.1(C)-(D).

To evaluate this advancement, different T_2^* volumes were acquired on a phantom and a healthy volunteer at 3T using a 64-channel head/neck coil array, paired with additional ΔB_0 field maps. All acquisitions parameters are detailed in Tab.1. For in vivo scans, a Cartesian GRAPPA4-accelerated reference was also acquired to perform a retrospective study, by simulating the B_0 inhomogeneities[4] using the acquired field map (Fig.2). On the phantom, volumes were collected in standard conditions with low artifacts (Fig.3(1)), then B_0 inhomogeneities were added by degrading the machine B_0 shimming (Fig.3(2)).

All image reconstructions were performed using the self-calibrated approach[3] and implemented in `pysap-mri`.[5]

Table 1: All acquisition parameters used in the phantom and in vivo studies.

Acquisitions / Parameters	**SPARKLING & MORE-SPARKLING**	**Cartesian GRAPPA4**	**ΔB_0 field map**
Field of view	$230 \times 230 \times 124.8$ mm^3		
Resolution	0.6 mm iso	0.6 mm iso	2 mm iso
Acquisition time	3 min 22 s	15 min 13 s	2 min 43 s
Echo time(s)	20 ms	20 ms	4.92 ms / 7.38 ms
Repetition time	37 ms	37 ms	703 ms
Dwell time	2 µs	5 µs	10 µs
Number of spokes	5329	19968	7296
Acceleration factor	15	4	-

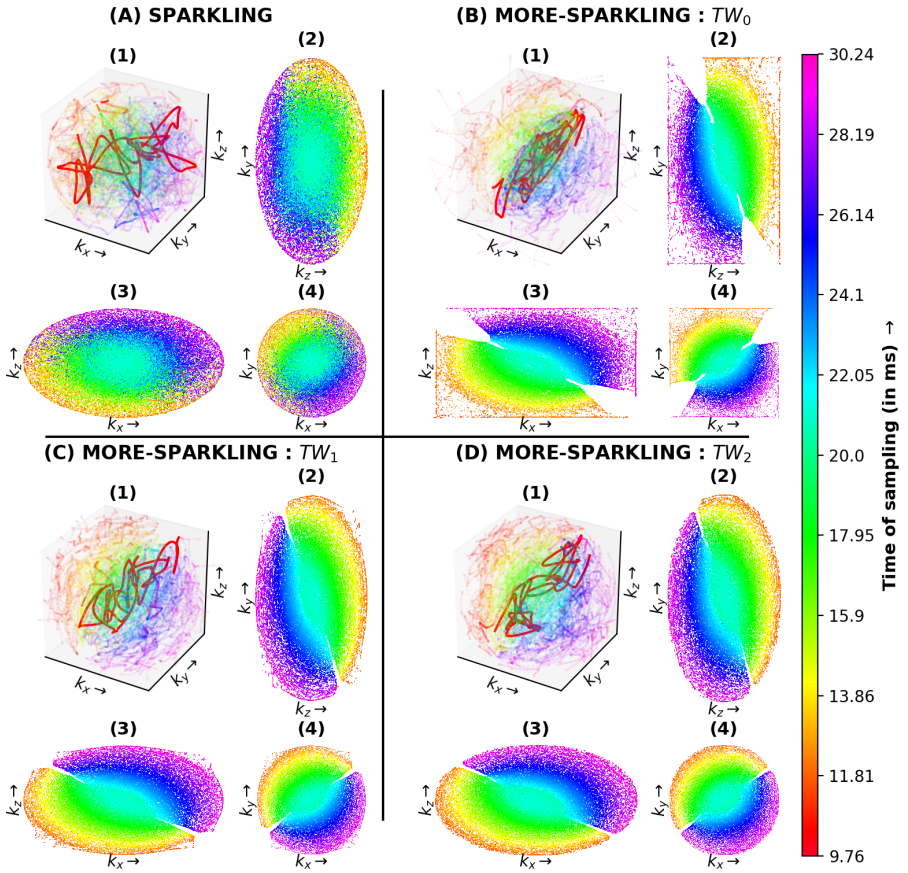

Figure 1: Comparison of different SPARKLING trajectories generated with $N_c = 5329$ (AF=15), $N_s = 2048$: (A) Without temporal weights, (B) with TW_0, (C) with TW_1, and (D) with TW_2. In each case, the 3D sampling pattern is shown in (1) and the mid-plane k-space slices along (2) k_x-axis, (3) k_y-axis and (4) k_z-axis. A rainbow coloring scheme overlays the sampling trajectories to encode the time in k-space samples.

4 Results

The retrospective study on a volunteer (Fig.2) shows a quality peak for TW_1 with an improved PSNR by 3dB compared to the original SPARKLING. Aside from sensitivity and registration differences, the retrospective study shows realistic B_0 inhomogeneity simulation compared to prospective in vivo acquisitions (Fig.4). While TW_1 brings better k-space coverage than TW_0, as visible in Fig.1 (B1, C1), TW_2 mostly shows a less mitigated impact of ΔB_0 artifacts (red/yellow arrows).

The prospective study on the phantom (Fig.3) shows significant improvements over B_0 inhomogeneities with temporal weights (blue arrows), decreasing with TW_1 and TW_2 (red arrows). However, without inhomogeneities TW_0 shows slightly degraded quality (B1, yellow arrows) over other trajectories. Similar results are observed in vivo (Fig.4) with more signal for MORE-SPARKLING in ΔB_0 regions (blue arrows). Importantly, sharper details and a cleaner contrast are recovered using TW_1 (E, red/yellow arrows). Overall, TW_1 shows improvements over TW_0 that can be attributed to balanced repulsion and reduced k-space holes.

5 Conclusion

In this work, we present a significant advancement to the SPARKLING formulation which takes the temporal nature of the signal acquisition into account, resulting in MORE-SPARKLING trajectories that exhibit reduced ΔB_0 artifacts.

However, our first proposition to tackle this problem resulted in the apparition of k-space holes during the optimization process due to increased repulsion. Although we addressed this issue by disabling the temporal weighting prior to the final decimation step, more generic solutions could be achieved by further improving further the formulation. These aspects will be addressed in future works.

Acknowledgements

The concepts and information presented in this article are based on research results that are not commercially available. This work was granted access to the HPC resources of IDRIS under the allocation 2021-AD011011153 made by GENCI. Chaithya G R was supported by the CEA NUMERICS program, which has received funding from the European Union's Horizon 2020 research and innovation program under the Marie Sklodowska-Curie grant agreement No 800945.

References

[1] G R Chaithya et al. Optimizing full 3D SPARKLING trajectories for high-resolution T2*-weighted Magnetic Resonance imaging. *under review* at *IEEE Transactions on Medical Imaging*, May 2021.

[2] G. Daval-Frérot et al. Off-resonance correction for non-Cartesian SWI using internal field map estimation. In *29th Proceedings of the ISMRM society*, number 3551, virtual, May 2021.

[3] Loubna El Gueddari, Carole Lazarus, Hanaé Carrié, Alexandre Vignaud, and Ph Ciuciu. Self-calibrating nonlinear reconstruction algorithms for variable density sampling and parallel reception mri. In *2018 IEEE 10th Sensor*

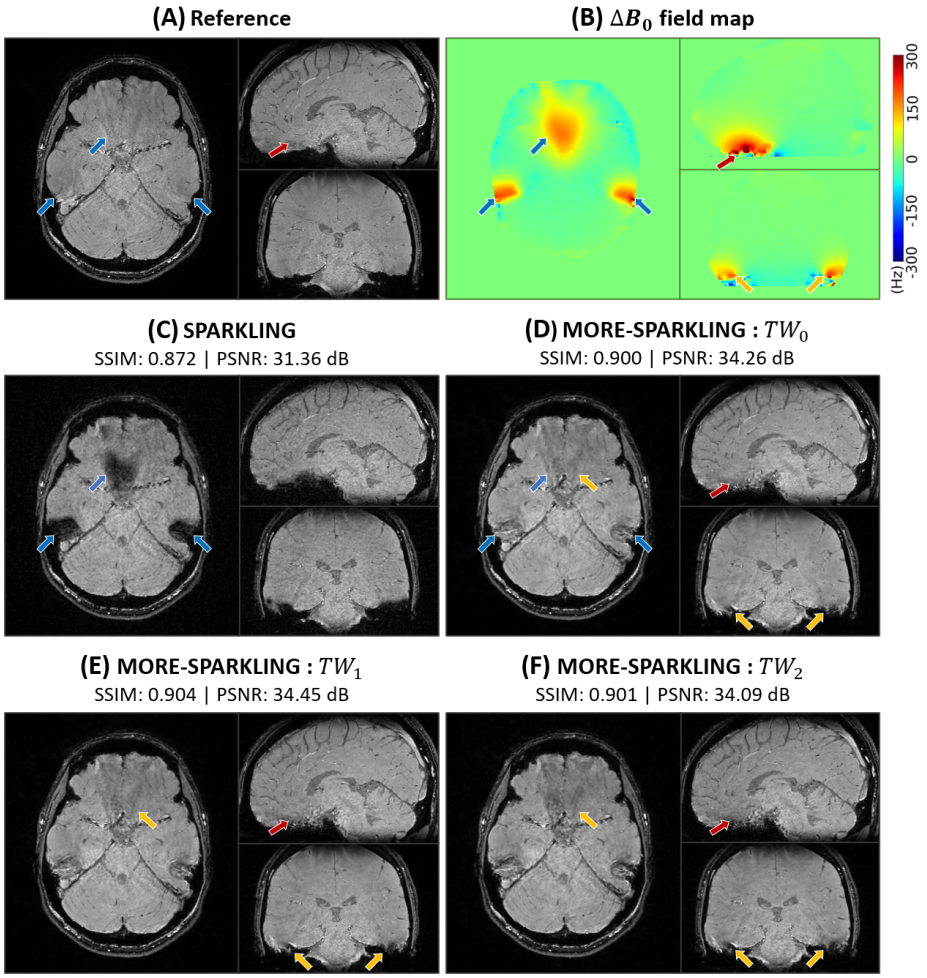

Figure 2: Retrospective study on healthy volunteer performed by projecting a Cartesian reference acquisition (A) and using the acquired ΔB_0 field maps (B) onto different SPARKLING trajectories : (C) Without temporal weights, (D) with TW_0, (E) with TW_1, and (F) with TW_2. The SSIM and PSNR scores are obtained by comparison with the Cartesian reference (A). Arrows are used to point out differences related to ΔB_0 blurring (blue), contrast (yellow) and anatomical details (red).

Array and Multichannel Signal Processing Workshop (SAM), pages 415–419. IEEE, 2018.

[4] Jeffrey A Fessler, Sangwoo Lee, Valur T Olafsson, Hugo R Shi, and Douglas C Noll. Toeplitz-based iterative image reconstruction for mri with cor-

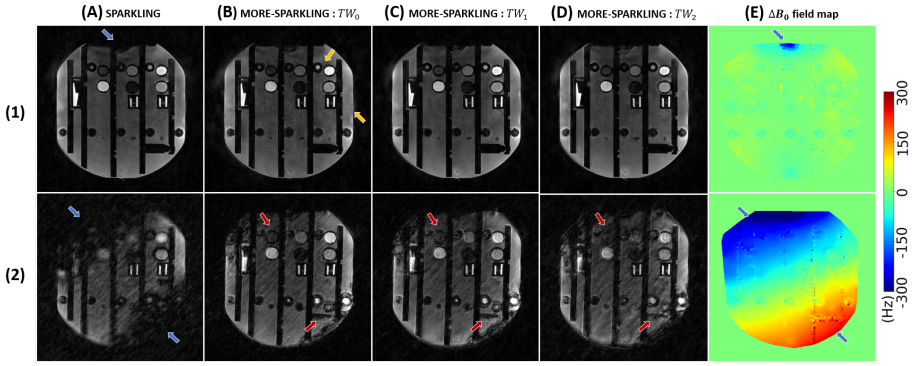

Figure 3: Prospective study on phantom comparing different SPARKLING trajectories : (A) Without temporal weights, (B) with TW_0, (C) with TW_1, and (D) with TW_2. All sampling patterns are presented with (1) a complete B_0 shimming and (2) with a purposely degraded B_0 shimming, resulting in inhomogeneities visible on the ΔB_0 field maps (E). Arrows are used to point out differences related to ΔB_0 blurring (blue), contrast (yellow) and shape details (red).

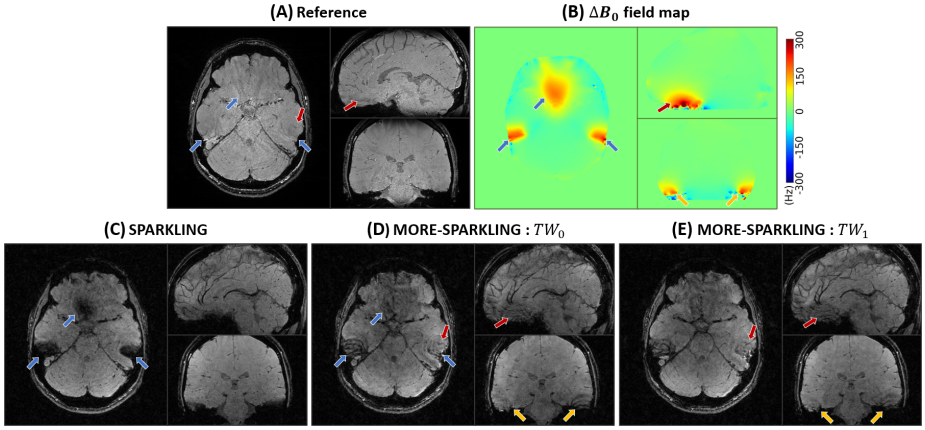

Figure 4: Prospective study on healthy volunteer comparing (A) a Cartesian reference with different SPARKLING trajectories : (C) Without temporal weights, (D) with TW_0 and (E) with TW_1. The B_0 field inhomogeneities are visible on the acquired ΔB_0 field maps (B). Arrows are used to point out differences related to ΔB_0 blurring (blue), contrast (yellow) and anatomical details (red).

rection for magnetic field inhomogeneity. *IEEE Transactions on Signal Processing*, 53(9):3393–3402, 2005.

[5] Loubna El Gueddari et al. PySAP-MRI: a Python Package for MR Image Reconstruction. In *ISMRM WS on Data Sampling and Image Reconstruc-*

tion, Sedona, AZ, United States, January 2020.

[6] C. Lazarus et al. SPARKLING: variable-density k-space filling curves for accelerated T2*-weighted MRI. 81(6):3643–3661, 2019.

[7] C. Lazarus et al. 3D variable-density SPARKLING trajectories for high-resolution T2*-weighted magnetic resonance imaging. 2020.